Materials Research Proceedings **32** (2023) 72-80 https://doi.org/10.21741/9781644902615-7

Superplasticity of Ti-6Al-7Nb alloys with different initial microstructures processed by high-pressure torsion

Kathy González Jiménez[1,a], Joaquín E. González Hernández[1,b], Jorge M. Cubero-Sesin[1,c*] Jeremy Barrantes Rodríguez[1,d] and Zenji Horita[2-4,e]

[1]Centro de Investigación y Extensión en Materiales (CIEMTEC), Escuela de Ciencia e Ingeniería de los Materiales, Instituto Tecnológico de Costa Rica, Cartago 159-7050, Costa Rica

[2]Graduate School of Engineering, Kyushu Institute of Technology, Kitakyushu 804-8550, Japan

[3]Magnesium Research Center, Kumamoto University, Kumamoto 860-8555 Japan

[4]Synchrotron Light Application Center, Saga University, Saga 840-8502, Japan

[a]kathygon18@estudiantec.cr, [b]jegonzalez@itcr.ac.cr, [c]jcubero@itcr.ac.cr, [d]jerbara1@estudiantec.cr and [e]horita.zenji.688@m.kyushu-u.ac.jp

Keywords: High-Pressure Torsion, Ultrafine Grained, Nanostructure, Superplasticity, Strain Rate Sensitivity, Activation Energy

Abstract. Ti-6Al-7Nb alloy was quenched below and above the β-phase field and processed by high-pressure torsion (HPT) to produce different grain sizes in the ultra-fine range. The influence of temperature and strain rate over the superplastic properties, activation energy and strain rate sensitivity were evaluated by high temperature tensile tests. The mechanical properties were complemented with Vickers microhardness measurement of heat treated and HPT-processed samples. The crystallographic analysis was performed through XRD and EBSD studies in the grip and tip of the high temperature tensile specimens. Microhardness measurements show significant hardening with respect to the imposed strain after HPT. Meanwhile, high superplastic elongation of 1200% was accomplished at 850 °C with a strain rate of $2x10^{-3}$ s^{-1}. EBSD studies of the failed specimens suggest that the tip part exhibited dynamic recrystallization during tensile test, which produced a larger grain size of ~5.1 μm and higher fraction of β phase of 3.7%, with respect to the grip part under static recrystallization, which attained ~3.4 μm grain size and 3.3% β phase fraction.

Introduction

Titanium alloys are widely used in aerospace industry and medical implants due to their workability [1–3], low density (60% of steel), thermal stability, high mechanical and corrosion resistance [4–7]. Titanium alloys are classified according to their crystal structure with respect to the presence of phases: α (HCP), β (BCC) and duplex α+β [4–7]. The α+β alloys have enough content of β-stabilizer to allow the nucleation of β-phase particles at room temperature, these duplex microstructures provide balanced properties and can be modified through heat treatments (increases strength 30% to 50% in comparison with annealed condition or overaged) [7]. Ti-6Al-7Nb is an α+β alloy with enough Nb content to produce a microstructure that can serve as replacement to the commonly used Ti-6Al-4V alloy, and avoid the toxicity associated with V^+ ion release [1–7]. On the other hand, superplastic properties of metals and alloys provide an excellent option for fabrication of parts with complex shape at lower temperatures and higher strain rates than conventional hot working, which results in lower energy consumption [8]. Superplasticity is characterized by high elongation to failure (above 400%) during a high temperature tensile test [9]. Superplastic behavior requires three main conditions: (1) high deformation temperature $T > 0.5T_m$ (T_m: melting temperature), (2) grain size < 10 μm and (3) low strain rate, in the order of

10^{-3} to 10^{-5} s^{-1} [10–11]. The strain rate sensitivity index, *m*, describes the capability of plastic deformation. It has been observed that superplastic flow requires m ~ 0.5 [12–14]

Eq. 1 shows the constitutive equation for superplastic behavior of microcrystalline materials, equation used to find the activation energy of the process [13–15].

$$\dot{\varepsilon} = A\left(\frac{b}{d}\right)^{P}\left(\frac{\sigma}{G}\right)^{n} e^{\frac{-Q}{RT}} \quad (1)$$

Where $\dot{\varepsilon}$ is the strain rate, A is a dimensional constant, b is the Burger vector, d is the grain size, P is the inverse exponent of the grain size, σ is the yield stress, G is the shear modulus of elasticity, n = 1/m, and $e^{-Q/RT}$ denotes the grain boundary diffusion coefficient, where Q is the activation energy, R is the ideal gas constant and T is the temperature. Eq.1 can be rewritten in such a way that it becomes a linear equation, as shown by Eq. 2 [13–15].:

$$\ln \dot{\varepsilon} = \ln\left[A\left(\frac{b}{d}\right)^{P}\left(\frac{\sigma}{G}\right)^{n}\right] - \frac{Q}{R}T^{-1} \quad (2)$$

Severe Plastic Deformation (SPD) methods are an excellent option for producing nanostructured alloys with enhanced properties. SPD processing can be described as metal forming techniques that induce large shear strains under high hydrostatic pressure at low temperatures (commonly less than 0.4T melting temperature), capable of producing ultrafine grained (UFG) structures [16–21]. The most effective methods to produce grain refinement is High-Pressure Torsion (HPT) [17–20], in which a disc is subjected to torsional straining under a high hydrostatic pressure. Several studies reported the superplastic elongation in titanium alloys: 987% in Ti55 alloy [22], a range between 768% and 2100% for Ti-6Al-4V [23–25] and 820% for UFG Ti-6Al-4V[26]. UFG Ti-6Al-7Nb produced by HPT attained 930% [27] and 400% [28] of superplastic elongation. This work describes the influence of strain rate and temperature over the superplastic properties of nanostructured Ti-6Al-7Nb produced by quenching and HPT, through the calculation of strain rate sensitivity (m) and activation energy (Q).

Experimental procedures

Discs of 10 mm in diameter and 1.5 mm in thickness were sliced from commercial Ti-6Al-7Nb bar by electrical discharge machining (EDM). Then the specimens were subjected to heat treatment at 700°C for 2 h in air atmosphere and cooled in cold water. The cooling in cold water from 700 °C did not have a major effect in the microstructure of a slowly cooled Ti-6Al-7Nb, so it is referred to as annealed condition (A). Following, samples were heat treated at 1060°C (which is above β-transus) above martensite start (Ms) for 1 h and quenched in cold water. This condition is referred to as quenched (Q). HPT was conducted on 10 mm diameter discs from A and Q conditions at room temperature, under 6 GPa for N = 10 revolutions at ω = 1 rpm. Vickers microhardness measurements were performed with 500 μm spacing in radial directions from the center of the disc for: annealed (A), annealed+quenched (A+Q) and annealed, quenched and HPT-processed samples (A+Q+HPT). Tensile test specimens were also extracted by EDM from a location 2 mm from the center of the 10 mm disc. The dimensions of the gage section were 1.5 mm length, 0.7 mm width and 0.5-0.7 mm thickness, as shown schematically in the inset of Fig. 4. High temperature tensile tests were conducted in air atmosphere combining temperatures of 700 °C, 750 °C, 800 °C, 850 °C and 900 °C with initial strain rates of $1x10^{-3}$ s^{-1}, $2x10^{-3}$ s^{-1}, $5x10^{-3}$ s^{-1}, $1x10^{-2}$ s^{-1} and $2x10^{-2}$ s^{-1}. These tests allowed the calculation of strain rate sensitivity (m) and activation energy of Ti-6Al-7Nb for comparison with reported literature and stablish the deformation mechanism during tensile test.

Materials Research Proceedings **32** (2023) 72-80 https://doi.org/10.21741/9781644902615-7

Metallographic analysis was performed in optical microscope for annealed and quenched conditions, the discs were polished to a mirror-like finish and etched with Kroll´s reagent. X-ray diffraction (XRD) was carried out to identify the main phases in heat treated, HPT-processed and failed tensile specimen samples, using Cu-Kα radiation (λ = 1.54016 Å), scanning step of 0.02° and speed of 1°/min. Transmission electron microscopy (TEM) observations were carried out at 200 kV from 3 mm discs extracted from the periphery of the HPT-processed disks, thinned by twin-jet electropolishing in a solution of 90% acetic acid and 10% perchloric acid under 20 V. After high temperature tensile test, the failed specimens were selected for crystal structure and phase fraction analysis using electron backscatter diffraction (EBSD) in grip and tip sections. EBSD samples were mechanically polished to a mirror-like finish followed by electropolishing using the same electrolyte and conditions as for the TEM specimens.

Results and discussion

Fig. 1a shows the initial microstructure after annealing at 700 °C, which is a typical α+β microstructure, consisting of equiaxed grains of α-phase with β-phase particles at grain boundaries. Fig. 1b shows the as-quenched condition from 1060 °C, which consists of a combination of α grains with regions of basket-weave structure of acicular martensite α´ and β platelets. β-transus temperature for Ti-6Al-7Nb is 1010 °C, thus quenching from 1060 °C allowed the formation of the martensitic structures [29].

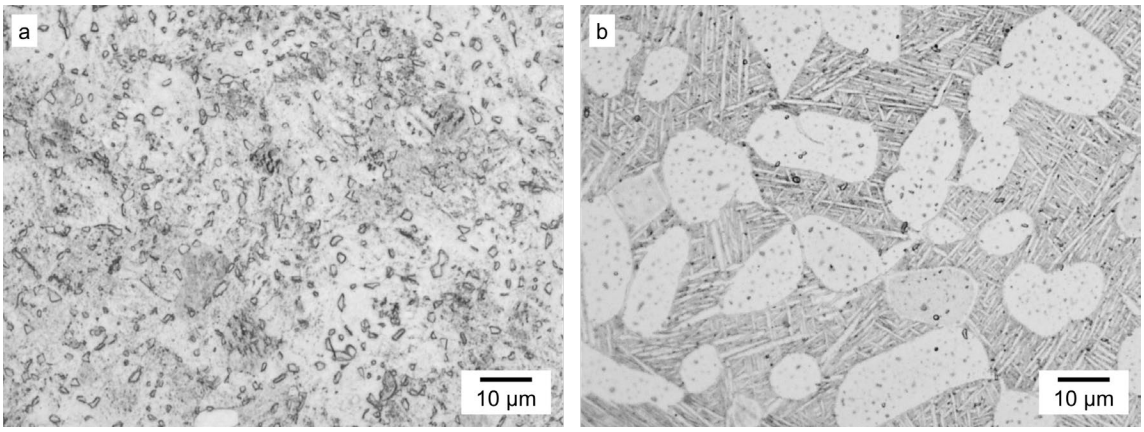

Fig. 1. *Ti-6Al-7Nb microstructures after (a) annealed at 700°C and (b) quenched in cold water from 1060°C.*

Fig. 2 shows a comparison of XRD profiles of A, A+HPT, A+Q, A+Q+HPT conditions, as well as the tip and grip section of A+Q+HPT specimens tested at 850°C with strain rate of $2x10^{-3}$ s^{-1}. Peaks of α and β are observed in A sample. The intensity of the β-phase peaks is decreased beyond the resolution of the XRD for A+HPT sample, which is associated with the refinement of the β-phase particles by HPT. The A+Q and A+Q+HPT samples, show similar behavior, in this case also associated with the fine β platelets that are part of the martensitic structure formed by quenching. The presence of α´ is overlapped with the α peaks in these cases as well. Increased peak broadening can be observed in the cases after HPT processing due to grain refinement and high density of lattice defects [16-18]. The A+Q+HPT tip and grip section profiles show the presence of both α and β peaks with less peak broadening due to the recrystallization and grain growth that occurs during high temperature tensile test.

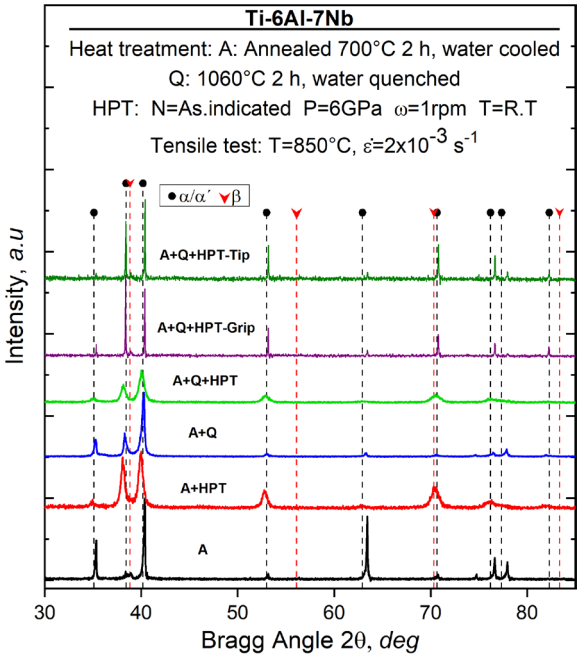

Fig. 2. *XRD profiles before and after HPT and after tensile testing*

Fig. 3 shows Vickers microhardness profiles of A, A+Q, A+HPT and A+Q+HPT samples with respect to the distance from the center of the discs. Dotted lines correspond to the hardness levels of the microstructures in the initial states (after heat treatment: A and A+Q). The A+Q sample attained higher hardness than A, since the resulting microstructure is finer [24]. After HPT, both conditions A+HPT and A+Q+HPT exhibited an increase in microhardness up to ~350 HV and ~400 HV in the edge of the disc respectively, strongly associated with grain refinement provided by HPT. Examination of TEM images also shown in Fig. 3, reveal that the A+Q+HPT had a smaller grain size with respect to A+HPT, it was estimated ~50-70 nm from dark-field images.
High temperature tensile test results are shown in Fig. 4a for the case of A+Q+HPT samples tested at an initial strain rate of $2x10^{-3}$ s^{-1}. This strain rate attained the highest elongations at any given temperature, but in general all samples processed by HPT attained superplastic elongation > 400%, when tested at 800 °C or higher, as shown by selected samples in Fig. 4b. Superplastic elongation increased with testing temperature at the expense of yield stress. Superplastic elongation of A+Q+HPT samples between 800 °C and 900 °C increased from 700% up to 1200% with maximum magnitude reached at 850 °C with a strain rate of $2x10^{-3}s^{-1}$. Meanwhile, A+HPT samples tested at 850°C with $2x10^{-3}$ s^{-1} strain rate reached 900% elongation. This suggests there are differences in microstructural evolution and grain refinement from the initial microstructures. Tensile test at 700°C with a strain rate of $1x10^{-2}$ s^{-1} exhibited the lowest elongation, with not much difference with respect to the quenching.

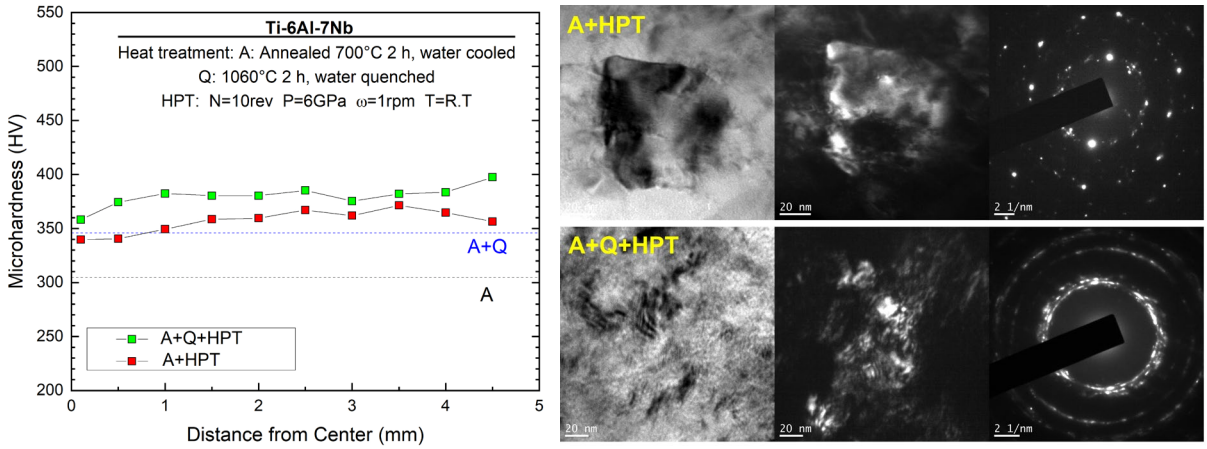

Fig. 3. *Vickers microhardness (left) and TEM bright-field, dark-field, SAED images (right) of heat-treated samples after HPT processing.*

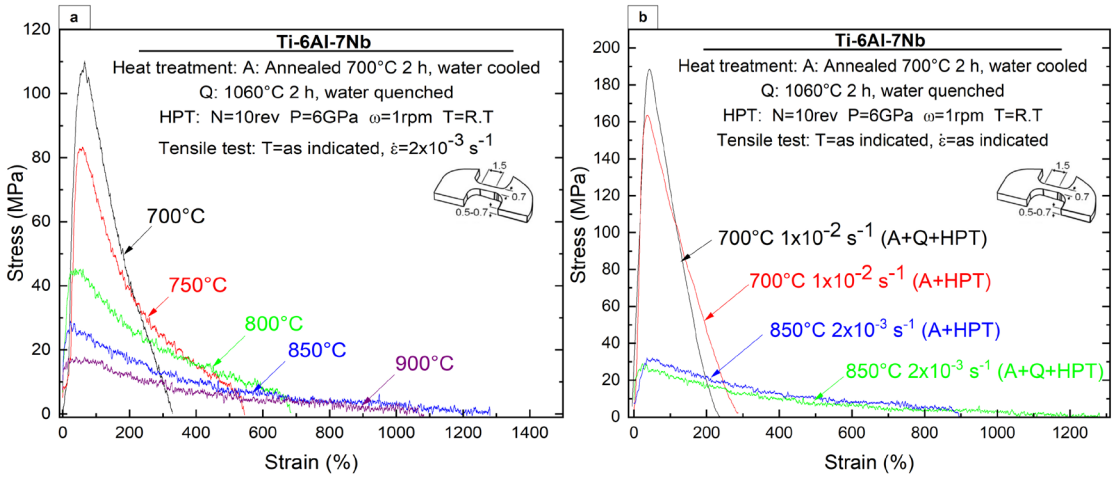

Fig. 4. *Stress-strain curves at different temperatures and strain rates: a) A+Q+HPT at a strain rate of $2x10^{-3}$ s^{-1} and b) A+HPT and A+Q+HPT at 700°C and 850°C at a strain rate of $1x10^{-2}$ s^{-1} and $2x10^{-3}$ s^{-1} respectively*

Fig. 5a shows the plot for maximum stress versus initial strain rate of each of the testing temperatures using logarithmic scale. The best fit lines were estimated for each temperature and consequently the strain rate sensitivity parameter was estimated as the slope of each line $m = (\partial ln\sigma/(\partial ln\dot{\varepsilon})_{\varepsilon,T}$. The values obtained were: 0.275, 0.342, 0.390, 0.388 and 0.462 for 700°C, 750°C, 800°C, 850°C and 900°C respectively. These values are very close to usual magnitudes observed in superplastic region of titanium alloys with m ≥ 0.3 and the grain boundary sliding deformation mechanism [13,25].

Fig. 5b. shows the plot of initial strain rate in logarithmic scale against the inverse of the temperature. Following Eq. 2, the data were adjusted to a linear plot in terms of $\ln(\dot{\varepsilon})$ vs T^{-1}, with σ constant so that the activation energy associated with the process can be obtained from the slope of the fitted line. For the A+Q+HPT samples, the activation energy achieved 277.89 ± 24.15 kJ/mol. This result is slightly higher than 174 kJ/mol which is ordinarily obtained for Ti-6Al-4V α+β alloys [24,30], above self-diffusion of α and β Ti (169 and 153 kJ/mol respectively [30]) and still below the activation energy for dislocation displacement deformation of α and β Ti (306 and 317 kJ/mol respectively [30]). All this suggests that the deformation process present is driven mainly by grain boundary sliding, with a higher activation energy than reported, probably due to

Materials Research Proceedings **32** (2023) 72-80 https://doi.org/10.21741/9781644902615-7

other processes that are occurring simultaneously to grain boundary sliding, such as dynamic recrystallization and dislocation accommodation.

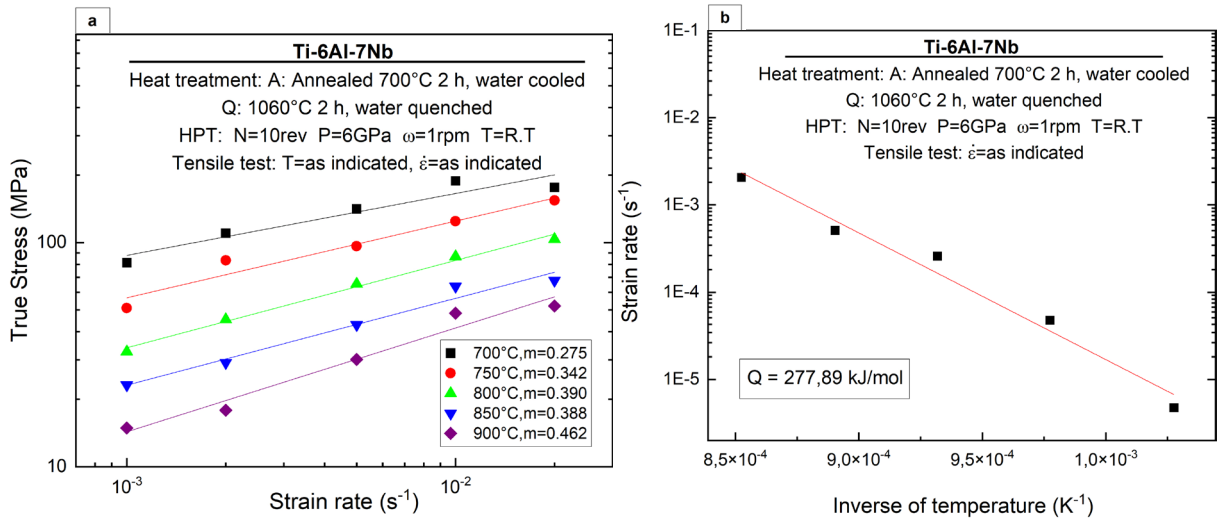

Fig. 5. *Linear fit of (a) maximum stress versus initial strain rate in tensile tests at different temperatures and of (b) initial strain rate versus inverse of temperature*

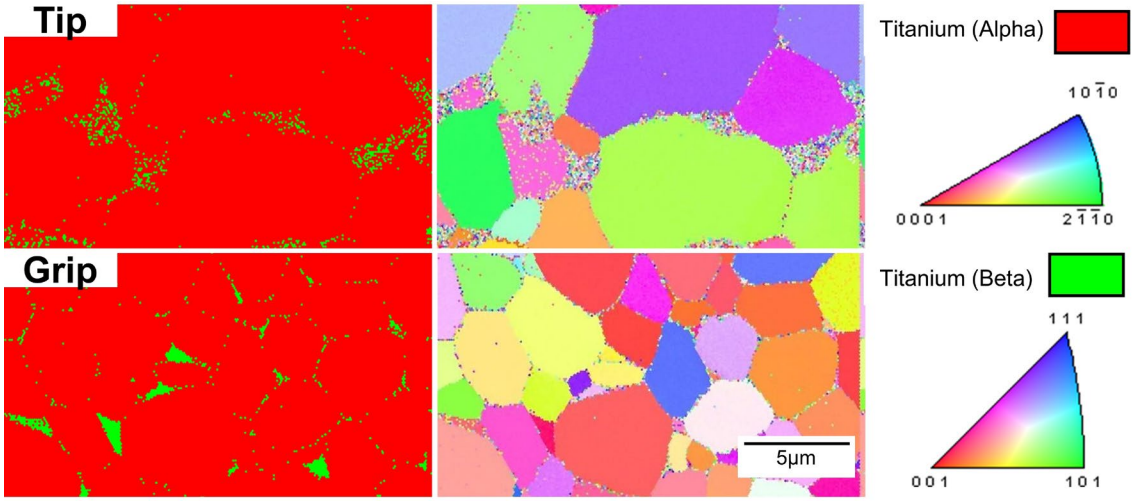

Fig. 6. *EBSD for sample A+Q+HPT after tensile stress at 850°C with strain rate of $2x10^{-3}$ s^{-1}.*

EBSD analysis was performed in the grip and tip sections of the A+Q+HPT specimen after the high-temperature tensile test at 850°C and strain rate of $2x10^{-3}$ s^{-1}. Fig. 6 shows the corresponding phase and orientation mapping results. The tip region exhibited a larger grain size ~5.1 μm when compared to the grip region of ~3.4 μm, suggesting that the tip part is subjected to dynamic recrystallization during tensile test, and thus higher energy is generated in the fault zone to allow the grain growth compared to the non-deformed zone, as well as recrystallization of a higher fraction of β phase of ~3.7%, with respect to the grip part of ~3.3%. Therefore, the accommodation mechanisms generated when the A+Q+HPT nanostructure recrystallizes to a typical α+β structure during tensile test can explain the higher activation energy and increased superplastic elongation with respect to the A+HPT condition.

Summary
In this work, Ti-6Al-7Nb alloy was heat treated in two conditions and processed through HPT to produce ultrafine-grained structures. Duplex α+β microstructure was observed in annealed condition and combination of α grains with regions of acicular grains of martensite α′+ β in quenched condition. After HPT processing, both conditions A+HPT and A+Q+HPT exhibited an increase of microhardness measurements up to ~350 HV and ~400 HV. High temperature tensile tests were conducted at different temperatures and strain rates to calculate activation energy and strain rate sensitivity. Superplastic elongation of nanostructured Ti-6Al-7Nb reached 900% and 1200% for A+HPT and A+Q+HPT samples, respectively with a strain rate of $2x10^{-3}$ s^{-1} at 850°C. Activation energy of A+Q+HPT was calculated (277.89 ± 24.15) kJ/mol which suggests grain boundary sliding is not the single deformation mechanism assisting the superplastic elongation. EBSD analysis suggest the occurrence of dynamic recrystallization during tensile test in the tip of failed tensile test specimen, which resulted in larger grain size with respect to the grip part. Thus, accommodation of deformation is enhanced by the finer initial microstructure by quenching which is refined to smaller grains by HPT processing when compared to the annealed initial condition.

References

[1] M. Niinomi, Mechanical biocompatibilities of titanium alloys for biomedical applications, J. Mech. Behav. Biomed. Mater. 1 (2008) 30-42. https://doi.org/10.1016/j.jmbbm.2007.07.001

[2] M. Balazic, J. Kopac, M.J. Jackson, W. Ahmed, Review: titanium and titanium alloy applications in medicine, Int. J. Nano and Biomaterials. 1 (2007) 33-34. https://doi.org/10.1504/IJNBM.2007.016517

[3] A.S. Hoffman, Introduction, The Diversity and Versatility of Biomaterials, in: B.D. Ratner, A.S. Hoffman, F.J. Schoen, J.E Lemons (Eds.), Biomaterials Science, An Introduction to Materials: Third Edition, Elsevier, Oxford, 2013, pp. 63-64. https://doi.org/10.1016/B978-0-08-087780-8.00007-3

[4] F.H. Froes, Titanium: Physical Metallurgy, Processing, and Applications, ASM International, 2015. https://doi.org/10.31399/asm.tb.tpmpa.9781627083188

[5] M.J. Donachie, Titanium: A Technical Guide, second ed., ASM International, 2000. https://doi.org/10.31399/asm.tb.ttg2.9781627082693

[6] I. Polmear, D. StJohn, J.F. Nie, M. Qian, Titanium Alloys, in: I. Polmear, D. StJohn, J.F. Nie, M. Qian (Eds.), Light Alloys, Metallurgy of the Light Metals, Elsevier, 2017, pp. 369-460. https://doi.org/10.1016/B978-0-08-099431-4.00007-5

[7] S. Lampman, Titanium and Its Alloys for Biomedical Implants, in: R.J Narayan (Eds.), Materials for Medical Devices: Volume 23, ASM International, 2012, pp.223-236. https://doi.org/10.31399/asm.hb.v23.a0005674

[8] M. Naito, T.Yokoyama, M.Hosokawa, K. Nogi, Nanoparticle Technology Handbook, third ed., Elsevier, 2008

[9] T.G. Langdon, Seventy-five years of superplasticity: Historic developments and new opportunities, J. Mater. Sci. 44 (2009) 5998-6010. https://doi.org/10.1007/s10853-009-3780-5

[10] T.G. Langdon, Superplasticity of bulk nanostructured materials, in: M.J. Zehetbauer, Y.T. Zhu (Eds.), Bulk Nanostructured Materials, Wiley-VCH, Germany. 2009 pp.455-468. https://doi.org/10.1002/9783527626892.ch20

[11] Y.H.Z. Zhao, Advanced Mechanical Properties and Deformation Mechanisms of Bulk Nanostructured Materials, Trans. Tech. Publications, 2011.

[12] M.T. Pérez-Prado, M.E. Kassner, Superplasticity, in: M.E. Kassner (Eds), Fundamentals of Creep in Metals and Alloys, Elsevier, 2008: pp. 135-152. https://doi.org/10.1016/B978-0-08-047561-5.00006-3

[13] F.A. Mohamed, Micrograin superplasticity: Characteristics and utilization, Materials. 4 (2011) 1194-1223. https://doi.org/10.3390/ma4061194

[14] M. Kawasaki, T.G. Langdon, Principles of superplasticity in ultrafine-grained materials, J. Mater. Sci. 42 (2007) 1782-1796. https://doi.org/10.1007/s10853-006-0954-2

[15] A. Alhamidi, Z. Horita, Grain refinement and high strain rate superplasticity in alumunium 2024 alloy processed by high-pressure torsion, Mater. Sci. Eng. A. 622 (2015) 139-145. https://doi.org/10.1016/j.msea.2014.11.009

[16] R.Z. Valiev, R.K. Islamgaliev, I. V Alexandrov, Bulk nanostructured materials from severe plastic deformation, Prog. Mater. Sci. 45 (2000) 103-189. https://doi.org/10.1016/S0079-6425(99)00007-9

[17] R.Z. Valiev, Y. Estrin, Z. Horita, T.G. Langdon, M.J. Zehetbauer, Y.T. Zhu, Producing Bulk Ultrafine-Grained Materials by Severe Plastic Deformation, JOM. 58 (2006) 33-39. https://doi.org/10.1007/s11837-006-0213-7

[18] R.Z. Valiev, Y. Estrin, Z. Horita, T.G. Langdon, M.J. Zehetbauer, Y.T Zhu, Producing Bulk Ultrafine-Grained Materials by Severe Plastic Deformation: Ten Years Later, JOM. 68 (2016) 1216-1226. https://doi.org/10.1007/s11837-016-1820-6

[19] A. Azushima, R. Kopp, A. Korhonen, D.Y. Yang, F. Micari, G.D. Lahoti, P. Groche, J. Yanagimoto, N. Tsuji, A. Rosochowski, A. Yanagida, Severe plastic deformation (SPD) processes for metals, CIRP annals. 57 (2008) 716-735. https://doi.org/10.1016/j.cirp.2008.09.005

[20] A.P. Zhilyaev, T.G. Langdon, Using high-pressure torsion for metal processing: Fundamentals and applications, Prog Mater Sci. 53 (2008) 893-979. https://doi.org/10.1016/j.pmatsci.2008.03.002

[21] G. Faraji, H.S. Kim, H.T. Kashi, Severe Plastic Deformation: Methods, Processing and Properties, first ed., Elsevier, 2018. https://doi.org/10.1016/B978-0-12-813518-1.00003-5

[22] Z. Liu, P. Li, L. Xiong, T. Liu, L. He, High-temperature tensile deformation behavior and microstructure evolution of Ti55 titanium alloy, Mater. Sci. Eng. A. 680 (2017) 259-269. https://doi.org/10.1016/j.msea.2016.10.095

[23] G. Zhou, L. Chen, L. Liu, H. Liu, H. Peng, Y. Zhong, Low-temperature superplasticity and deformation mechanism of Ti-6Al-4V alloy, Materials. 11 (2018) 1212. https://doi.org/10.3390/ma11071212

[24] E. Alabort, P. Kontis, D. Barba, K. Dragnevski, R.C. Reed, On the mechanisms of superplasticity in Ti-6Al-4V, Acta Mater. 105 (2016) 449-463. https://doi.org/10.1016/j.actamat.2015.12.003

[25] J. Sieniawski, M. Motyka, Superplasticity in titanium alloys, JAMME. 24 (2007)123-130.

[26] W. Zhang, H. Ding, P.H.R. Pereira, Y. Huang, T.G. Langdon, Grain refinement and superplastic flow in a fully lamellar Ti-6Al-4V alloy processed by high-pressure torsion, Mater. Sci. Eng. A. 732 (2018) 398-405. https://doi.org/10.1016/j.msea.2018.07.010

[27] M. Ashida, P. Chen, H. Doi, Y. Tsutsumi, T. Hanawa, Z. Horita, Superplasticity in the Ti-6Al-7Nb alloy processed by high-pressure torsion, Mater. Sci. Eng. A. 640 (2015) 449-453. https://doi.org/10.1016/j.msea.2015.06.020

[28] J.M. Cubero-Sesin, J.E. Gonzalez-Hernandez, E. Ulate-Kolitsky, K. Edalati, Z. Horita, Superplasticity of nanostructured Ti-6Al-7Nb alloy with equiaxed and lamellar initial microstructures processed by High-Pressure Torsion, IOP Conf. Ser.: Mater. Sci. Eng. IOP Publishing, 194 (2017) 1-6. https://doi.org/10.1088/1757-899X/194/1/012041

[29] J. Sieniawski, W. Ziaja, K. Kubiak, M. Motyk, Microstructure and Mechanical Properties of High Strength Two-Phase Titanium Alloys, in: J. Sieniawski, W. Ziaja, K. Kubiak, M. Motyk (Eds), Titanium Alloys -Advances in Properties Control, InTech, 2013, pp.69-80 https://doi.org/10.5772/56197

[30] J. Shen, Y. Sun, Y. Ning, H. Yu, Z. Yao, L. Hu, Superplasticity induced by the competitive DRX between BCC beta and HCP alpha in Ti-4Al-3V-2Mo-2Fe alloy, Mater. Charact. 153 (2019) 304-317. https://doi.org/10.1016/j.matchar.2019.05.014